

Simulation and Analysis of Navigation Performance for Cislunar PNT Constellations

Mark Hartigan *

Georgia Institute of Technology, Atlanta, Georgia 30309.

Cislunar space currently lacks the navigation infrastructure from which Earth-centric space missions benefit – e.g. Global Navigation Satellite Systems (GNSS). The Deep Space Network is often used, but in recent years has become saturated with missions and scheduling time is becoming increasingly infeasible. Governments and national agencies such as the White House and NASA have identified a need for a scalable and interoperable positioning, navigation, timing, and communications (PNTC) service in cislunar space to support growing scientific interest and plans for a sustained human presence on the surface. This paper explores potential navigation methodologies and analytically determines achievable accuracy for such a system; navigation simulations are also conducted for example users on the lunar south pole – such as a ground station and lunar rover – to compare several different low-infrastructure constellation designs. Sufficient coverage of the south pole to yield navigation performance in the tens of meters is achieved for these users with as little as a four-satellite constellation.

I. Introduction

National and international interest is rapidly turning towards building a sustained human presence at the moon and in cislunar space. The White House Office of Science and Technology Policy has released a National Cislunar Science and Technology Strategy that identifies the need for scalable and interoperable cislunar positioning, navigation, timing, and communications (PNTC) capabilities to support NASA's Artemis program and beyond [1]. NASA's Moon-to-Mars architecture identifies this same need and is seeking comments and feedback on providing PNTC infrastructure for cislunar space [2]. NASA is currently in the early stages of developing such a cislunar constellation – called LunaNet – and has released details outlining the need for interoperability [3], while the European Space Agency has targeted the same need within their Moonlight Initiative [4].

Many organizations have agreed upon the need for a method by which users in cislunar space such as ground stations, rovers, astronauts, and orbiters can navigate in an efficient, accurate, and scalable way. Governmental organizations and private companies alike are identifying the solution to be a constellation of satellites broadcasting navigation signals similar to current Global Navigation Satellite Systems (GNSS). Such a constellation would permit users to derive

*Graduate Research Assistant, Space Systems Design Lab.

pseudorange measurements from these signals and thus trilaterate their position. Benefits of this proposed methodology are its ease of use and minimal hardware requirements for users, while also being near-infinitely scalable and capable of centimeter-level accuracy in Earth environments.

Georgia Tech Research Institute (GTRI) is sponsoring an internal research and development initiative within which the Space Systems Design Lab, Aerospace Systems Design Lab, and School of International Affairs are participating to make Georgia Tech competitive in this research field. This group is focused on developing the details of constellation geometry, signal design, achievable performance while ensuring adherence to all international policy agreements for a cislunar PNT architecture. Such a system will need to be rolled out in stages or phases due to the difficulties involved in launching to lunar orbits and the imminent need for a PNT service around the moon. Therefore, satellites should be deployed in such a way that extracts maximum utility from the placement of each satellite for the duration of its life. The work summarized within this report is focused on developing a modular and extensible software suite for evaluating the achievable navigation performance of a given satellite constellation; these results can then be used to inform an optimal constellation design at any stage of development.

II. Navigation Methodology

Given that navigation satellites – or nodes – are in orbit, how will a potential user derive useful navigation information from them? Two possibilities are *active* and *passive* ranging: in *active* ranging, a two-way communication link is established between the node and the user and information about the user’s position or other desired information is exchanged; in *passive* ranging, the node broadcasts some signal that the user can utilize to derive their own navigation solution. All current GNSS services use a form of passive ranging where users measure the time-of-flight of a navigation signal broadcast by the node to derive a pseudorange of the distance from the node to the user. This is the preferred navigation method to employ on a final cislunar constellation because of the theoretically infinite number of users that can be serviced simultaneously; however, it may be more desirable to employ active ranging methods using radio-frequency (RF) or optical communication links in early phases when satellite geometry cannot provide adequate coverage to all areas of the moon for pseudoranging purposes. Generally, RF signals have a wide beamwidth and can therefore reach multiple users at once without repositioning the antenna; optical links have a very narrow beamwidth and therefore can only service a single user at a time, but can achieve much higher data rates. This high bandwidth to a single target can be leveraged in satellite constellations as demonstrated by Giorgi et. al. [5] to synchronize clocks and transfer ephemeris data between nodes within the constellation, or to transfer data between the Earth and Moon on a dedicated link.

For a fully deployed PNT solution with global lunar coverage, the strongest candidate currently is to employ a GNSS-like service that utilizes radionavigation signals consisting of a carrier frequency modulated with a pseudo-random noise (PRN) code and pertinent navigation data. These PRN codes are unique to each satellite and repeat at fixed, well-defined intervals so by measuring the part of the PRN code received, the user can derive time-of-flight from

multiple nodes to triangulate their position. Making code measurements like these will be the primary focus of Section IV.C; more precise measurements can be made once a signal lock is acquired involving carrier phase measurements, which will be a focus of future work. Modulating a PRN code on the carrier frequency creates a spread-spectrum signal, which is beneficial for many reasons [6]: while the base signal is below the ambient RF noise floor, if the PRN code is known, the signal-to-noise ratio is very high; the autocorrelation properties of PRN codes mean that any multipath errors greater than one chip width are eliminated; and it is robust against radio frequency interference – among other benefits.

Another consideration is operating spectrum, or the carrier frequency of the navigation signal. For GPS, L1 operates at 1575.42 MHz and L2 operates at 1227.60 MHz. Generally, increasing carrier frequency decreases antenna beam width depending on antenna parameters. However, a higher carrier frequency (shorter cycle time) can also improve the achievable accuracy of carrier phase measurements. Currently, LunaNet has specified a carrier frequency of 2491.75 MHz [7] which conforms to the Space Frequency Coordination Group recommendation given in SFCG 32-2R4*. Analysis in the following sections will be focused on the currently-provided LunaNet specifications, though other frequencies may be examined in the future. Considerations must be made, though, so as to not interfere with planned radioastronomy on the far side of the moon and remain within recommendations of the SFCG. The far side of the moon is permanently hidden from the Earth, and therefore devoid of RF interference; this makes the far side invaluable for radio astronomy and is of high scientific interest to keep it interference-free. Current SFCG recommendations are using the 2483.5-2500 MHz band for dedicated PNT signals, while the 2025-2110 MHz and 2200-2290 MHz bands may be used for communications containing PNT ranging signals (all of the above fall into the IEEE S band of radio frequencies).

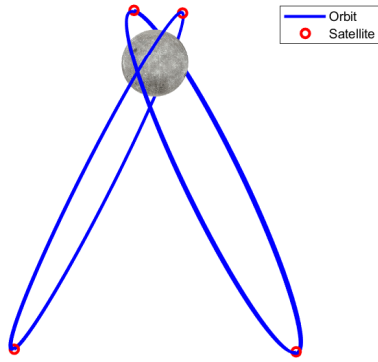
III. Constellation Evaluation

The purpose of this software utility is to provide the necessary tools to analyze constellations on the basis of navigation performance. To this end, this paper will explore several early-phase minimal constellations for navigation at the lunar south pole. The lunar south pole has been identified by NASA, the ESA, and others as a location of primary interest on the moon – mostly due to the existence of permanently sunlit regions and several craters that potentially contain water ice. Therefore, initial satellites deployed into this constellation would best be utilized by providing coverage to the lunar south pole. As this has been a recent topic of interest to the cislunar community, this paper will be analyzing two proposed constellations from literature and two novel designs in Section V.

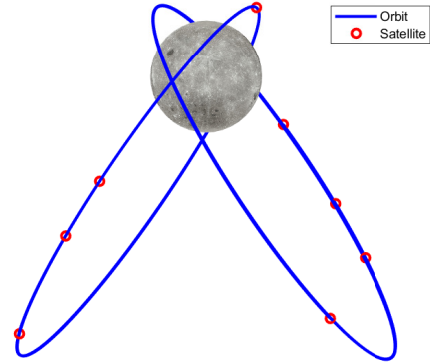
The first constellation explored is adapted Bhamidipati et al. [8], depicted in Figure 1a. This consists of two mirrored orbital planes, separated by a right ascension of 180° within which each satellite is separated by 180° . These orbits have an altitude of 9750.5 km, an eccentricity of 0.7, an inclination of 63.5° , and an argument of perilune of 90° .

The second constellation was conceived by Murata et al. [9], depicted in Figure 1b. Their work used two elliptical

*[https://www.sfcgonline.org/Recommendations/REC_SFCG_32-2R4_\(Freqs_for_Lunar_Region\).pdf](https://www.sfcgonline.org/Recommendations/REC_SFCG_32-2R4_(Freqs_for_Lunar_Region).pdf)



(a) 4-satellite constellation from [8].

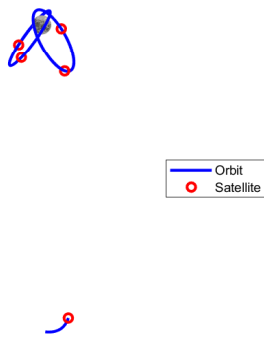


(b) 8-satellite constellation from [9].

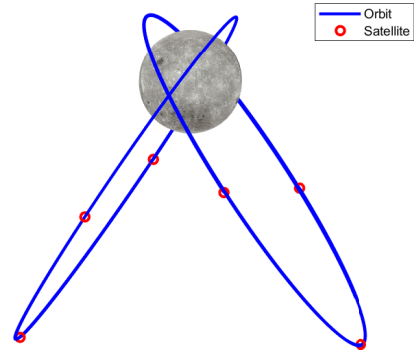
Fig. 1 Constellations from literature depicting orbit and spacing.

lunar frozen orbits (ELFOs) separated by a right ascension of 180° ; in one, each satellite is at a true anomaly of $90i^\circ$, $i = 0, 1, 2, 3$ and in the other $(45 + 90i)^\circ$, $i = 0, 1, 2, 3$. The selected orbits have a semimajor axis of 6541.4 km, eccentricity of 0.6, inclination of 56.2° , and argument of perilune of 90° .

The third constellation to be analyzed is an adaption of the first four-satellite constellation. It uses the same geometry but adds an additional satellite in a near-rectilinear halo orbit similar to that planned for use by the Lunar Gateway (Figure 2a). This new node will increase the number of visible satellites for long periods at a time due to its highly elliptical orbit, improving geometry and reducing dilution of precision.



(a) 5-satellite constellation.



(b) 6-satellite constellation.

Fig. 2 Novel constellations depicting orbit and spacing.

Finally, a six-satellite constellation is considered as an adaptation of the one proposed by Murata et al (Figure 2b). It maintains the same two mirrored orbital planes, but replaces the equispaced satellites with one string-of-pearls formation in each orbit, with the satellites following each other at true anomalies of 0° , 160° , and 200° . Navigation

simulations will be conducted comparing these four constellation geometries in Section V.

IV. User Navigation Error

A. Constellation Parsing

Satellite data is imported into simulations through provided data files with *a posteriori* discretized position data for each satellite in the constellation across the simulation period. Figure 3 shows the layout of one such data file, where each column corresponds to a different satellite and axis, while each row is a new time step.

Orbiter1.MoonInertial.X	Orbiter1.MoonInertial.Y	Orbiter1.MoonInertial.Z	Orbiter2.MoonInertial.X	...
0	1305.195533	2617.817248	0	...
-101.2681577	1304.735571	2616.894289	17.87302628	...
-202.4650648	1303.356688	2614.127424	35.74617133	...
-303.5197449	1301.061887	2609.522679	53.61936564	...
-404.3619493	1297.856143	2603.090038	71.49253974	...
...

Fig. 3 An example of a constellation data file.

This data can primarily be used to compute visible satellites for a given user and determine the dilution of precision (DOP) that results from the satellite geometry. DOP is a scale factor to quantify the effect that user-satellite geometry has on measurement uncertainty. Since there is uncertainty associated with the time of arrival – and therefore range measurement – of the pseudorange signal from each lunar navigation satellite, this creates a shell of uncertainty in three-dimensional space. If the line-of-sight vectors from the user to the navigation nodes are angularly close, the intersection of these shells creates a large region of uncertainty that isn't captured effectively with the user equivalent range error (UERE) discussed in Section IV.C. If the line of sight vectors are orthogonal, this intersection region is much smaller and thus the DOP is lower; a simple diagram of this concept is shown in Figure 4.

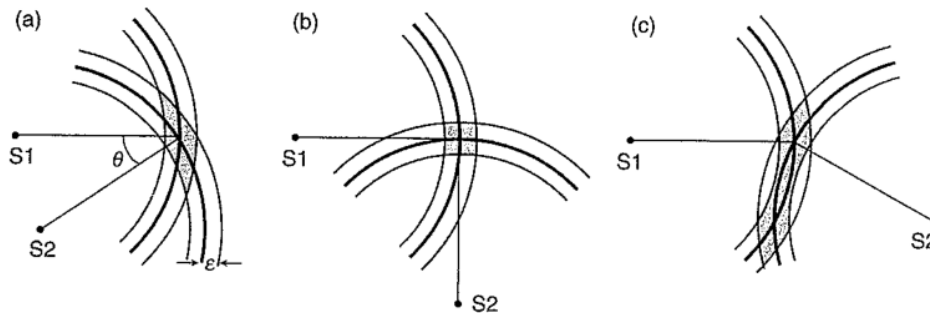


Fig. 4 A 2-D example of position estimation with range measurements [6, Chapter 6.1.2].

DOP can be broken into position dilution of precision (PDOP) and time dilution of precision (TDOP). These values

can be used in conjunction with the UERE to compute user navigation error:

$$\text{UNE} = \text{UERE} * \text{PDOP} \quad (1)$$

As seen in Equation (1), DOP applies a flat scale factor onto the UERE. Because of this, it is ideal to have the most satellites in view as possible, dispersed across the sky at a mix of high and low elevation angles. This software package calculates the DOP at each time step from the user's position for later use. If satellite k 's position is $\bar{x}_k = (x_k, y_k, z_k)$, $k \in [1, n]$ and the user's position is \bar{x}_0 , the DOP matrix is given by

$$H = (G^T G)^{-1}, \quad (2)$$

where

$$G = \begin{bmatrix} -\frac{1}{\|\bar{x}_1 - \bar{x}_0\|} \begin{bmatrix} x_1 - x_0 & y_1 - y_0 & z_1 - z_0 \end{bmatrix} & 1 \\ -\frac{1}{\|\bar{x}_2 - \bar{x}_0\|} \begin{bmatrix} x_2 - x_0 & y_2 - y_0 & z_2 - z_0 \end{bmatrix} & 1 \\ \dots & \dots \\ -\frac{1}{\|\bar{x}_n - \bar{x}_0\|} \begin{bmatrix} x_n - x_0 & y_n - y_0 & z_n - z_0 \end{bmatrix} & 1 \end{bmatrix} \quad (3)$$

An example of this software in action is shown in Figure 5, where number of visible satellites and PDOP was computed for simulated motion of the 8-satellite constellation above the lunar south pole.

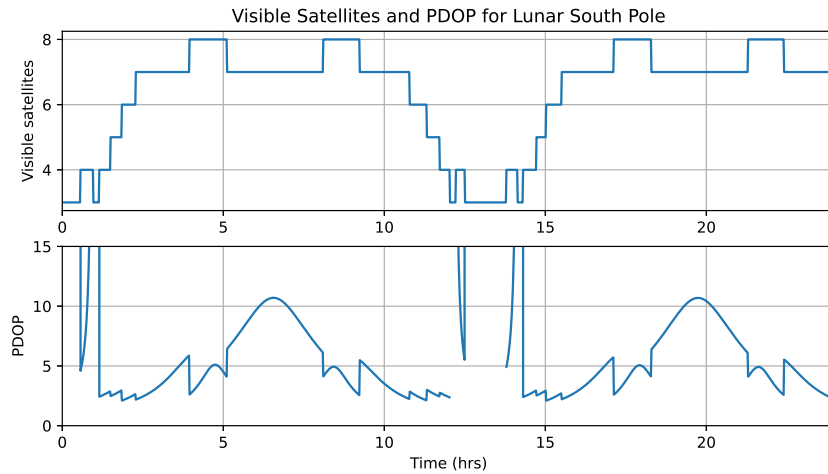


Fig. 5 24-hour simulated contacts of the 8-satellite constellation with the lunar south pole.

B. Clock Modeling

Navigation solution accuracy relies on the accuracy of both the broadcast node ephemerides (discussed in Section IV.C) and clock drift models. No clock is perfectly accurate with respect to a reference time: oscillators are subject to bias, drift, temperature effects, and random walk- and random jitter-type noise. For this reason, the GPS control segment regularly adjusts the onboard clocks in GPS satellites back to GPS Time; they also provide a model of clock drift in the form of polynomial coefficients. Clock drift at time t_1 can be characterized by Equation (4), where t_0 is the starting epoch, f_0 is the nominal oscillator frequency, Δf is the frequency bias, f is the frequency drift, and \tilde{f} is the oscillator noise.

$$\Delta t(t_1) = \Delta t(t_0) + \frac{\Delta f}{f_0}(t_1 - t_0) + \frac{f}{2f_0}(t_1 - t_0)^2 + \int_{t_0}^{t_1} \frac{\tilde{f}(t)}{f_0} dt \quad (4)$$

The U.S. Air Force's Global Positioning Systems Directorate regularly updates clock correction parameters in each satellite's navigation message providing the clock bias (a_0), clock drift (a_1), and clock drift rate (a_2) coefficients in Equation (5) below [10].

$$\Delta t(t_1) = a_0 + a_1(t_1 - t_0) + a_2(t_1 - t_0)^2 \quad (5)$$

Additionally, Figure 6 plots these corrections for a few sample satellites over two weeks. It is evident that the clock drift is largely driven by clock bias on the order of milliseconds, while the drift is less than a nanosecond per second and drift rate is roughly zero. According to the GPS Standard Positioning Service standards [11], the 95% statistical error from Coordinated Universal Time (UTC) shall never exceed 30 nanoseconds – and in practice is usually less than 7 [6, Chapter 5.6].

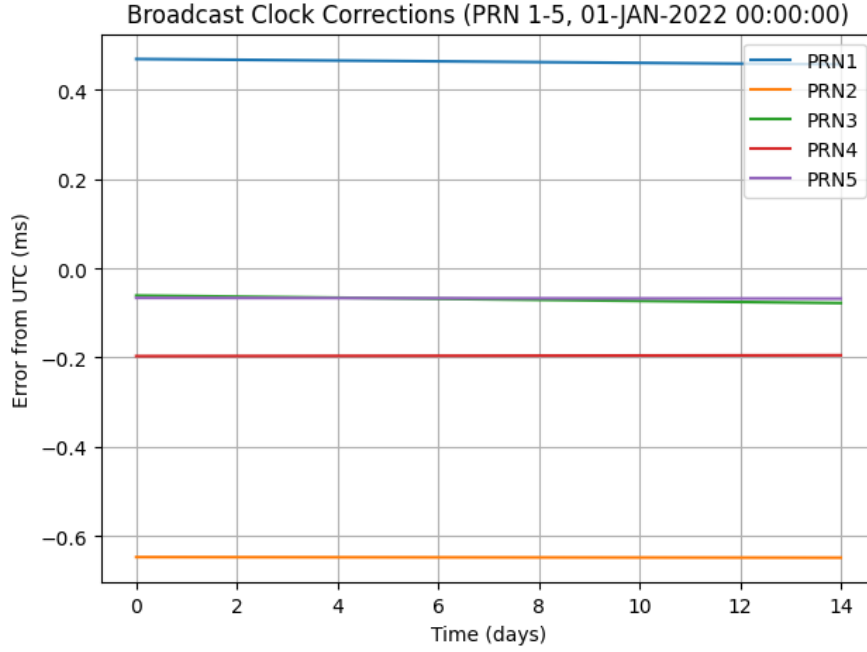


Fig. 6 Broadcast clock corrections from GPS satellites (PRN codes 1-5) on Jan 1, 2022.

However, the GPS ephemerides (as well as Galileo and GLONASS) do not attempt to model random noise, the final term in Equation (4). One way to account for random walk and random jitter noise is including in the error budget Hadamard variance $\sigma_H^2(\tau)$ [12], which estimates the relative frequency deviation of an oscillator due to random fluctuations over N intervals of length τ . The equation for Hadamard variance is

$$\sigma_H^2(\tau) = q_1\tau^{-1} + \frac{1}{6}q_2\tau + \frac{11}{120}q_3\tau^3 \quad (6)$$

From this equation, the RMS time error of the oscillator can be written as $\tau * \sigma(\tau)$, where τ is the time since the oscillator was last synchronized [6, Chapter 4.2.2]. Using the fitted models for a Rubidium Atomic Frequency Standard (RAFS) and Ultra-Stable Oscillator (USO) from [13], the 95% error is plotted in Figure 7. As shown, the 30-nanosecond standard set by GPS is quickly violated by a USO but takes around 11 days uncorrected from a RAFS for its uncertainty to rise above that threshold; to meet the 1-nanosecond performance GPS typically achieves, it would require accurate calibrations roughly twice daily.

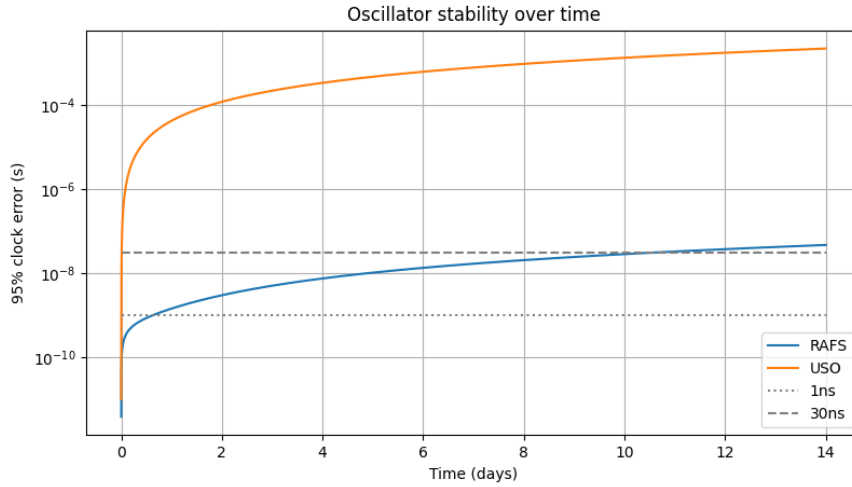


Fig. 7 Estimated 95% oscillator deviation over time.

This gives a general understanding of how clock synchronization and clock correction broadcasting should be considered when developing a navigation system. When selecting a clock, its stability is an important characteristic that sets the pace of updates required. A general approach would be to determine the accuracy standard to which the node clocks would be held, then set a correction schedule based on its stability. The most logical approach would be to update the nodes' onboard atomic clocks periodically from Earth using the precise timing standards already available. However, since this system would be operating in lunar orbit, regular updates from the Earth may be infeasible or undesirable from an operations perspective. One potential scheme – if budget is limiting – would be to provide a select few nodes with a more accurate but more expensive clock like a Cesium standard, then equip the rest with cheaper RAFS clocks and use the Cesium standards as truth. These standards would require a less rigorous correction schedule from more accurate clocks. Another option would be to arrive at a consensus between the nodes through some weighted maximum likelihood estimation of the true time, potentially extending time between required updates more. As lunar bases and stations are established in later phases, it may be possible to provide updates from the lunar surface and improve navigation performance through a more rigorous update schedule and better truth standard.

C. User Equivalent Range Error

Besides dilution of precision, the other variable required to calculate user navigation error discussed in Section IV.A is user equivalent range error (UERE). This differs from user range error (URE) which only considers signal-in-space errors, as UERE also approximates user receiver error.

Clock Errors

To address the consequences of the clock errors discussed in Section IV.B, the clock deviation σ_{clock} in seconds can

be transformed to meters by multiplying by the speed of light. Consequently, the 1- and 30-nanosecond thresholds become accumulated 95% position errors for the user of 0.3 and 9.0 meters, respectively. From these numbers it is evident that if sub-meter position accuracy is desired, clock errors must be kept below 3.3 nanoseconds at a minimum (assuming $PDOP = 1$).

Another idea worth considering, proposed by Giorgi et. al. [5] originally as an Earth-based GNSS solution, involves using communication links (optical, in this case) to synchronize clocks and ephemerides between satellites. They have posited that clock errors could be kept beneath 33 ps timing accuracy, yielding a sub-1 cm clock error. Their system involves placing the navigation nodes in MEO, with several satellites spread across a handful of orbital inclinations – similar to the ESA’s Galileo. Each orbital inclination would then have an associated satellite in LEO to provide constant line-of-sight communication with other parts of the constellation (pictured in Figure 8).

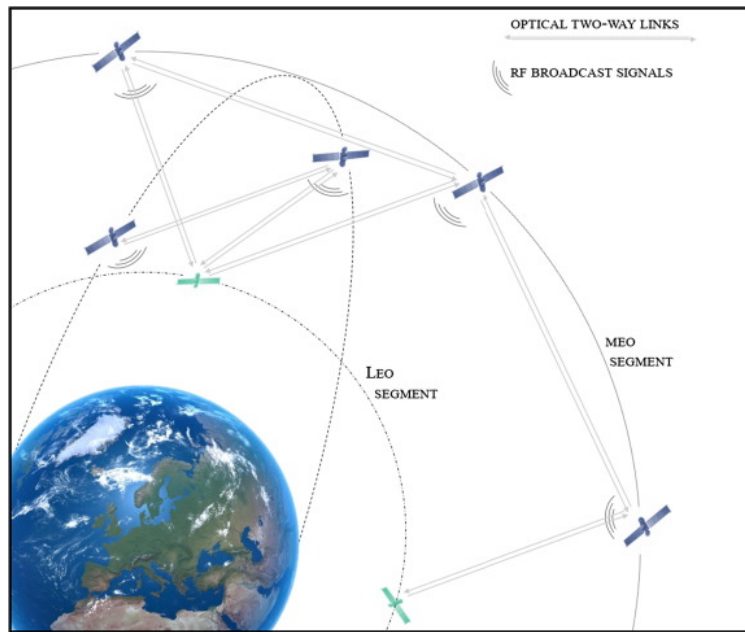


Fig. 8 MEO and LEO satellites carrying optical frequency references, connected by two-way optical links [5].

Orbit Determination Errors

Directly related to clock corrections are the node ephemerides, which in GPS are broadcast to the user to compute node positions for pseudorange measurements. In GNSS, these ephemerides are distributed by using ground station tracking to get a precise orbit determination (OD) solution, which is then uploaded into the satellite navigation message. In the lunar environment before any lunar stations are established, this OD solution will have to be computed onboard the nodes as there likely will not be enough resources available to track every node from the ground and update ephemerides daily. Therefore any satellite OD covariance will be passed along to the user – unless lunar ground stations for tracking are constructed in later phases. Small et. al. [13] have demonstrated that a lunar satellite is capable of achieving a mean

1σ RSS position error of approximately 3.7 meters using weak GNSS with outages, optical navigation ranging to the moon using center-finding, and a RAFS clock.

Receiver Noise and Multipath

Receiver noise and multipath errors are difficult to distinguish as they appear as very similar types of noise. Multipath errors arise from the radio signal arriving through an indirect path to the receiver. Luckily, due to the strong autocorrelation properties of PRN codes, any multipath errors greater than one chip width (around 59 meters based on current LunaNet specifications [7]) are eliminated. Multipath errors in GPS may range from 1 to 5 meters depending on if the environment is benign or highly reflective [6, Chapter 5.4.2].

Receiver noise is characterized by the following equation [6, Chapter 10.5]:

$$\sigma_{\Delta\tau} = cT_c \sqrt{\frac{d}{4TC/N_0}} \quad (7)$$

where c is the speed of light, T_c is the chipping time of the navigation signal, d is the receiver correlation spacing, T is the receiver averaging time, and C/N_0 is the signal power to noise spectral density ratio. According to LunaNet specifications, the planned chip width is 19.55 ns, which corresponds with a chipping rate of 5.115 Mcps [7]. The correlation spacing $d \in [0.1, 1]$ is the space between samples in the delay lock loop, and is commonly set to 0.1 to minimize noise – lower values do not yield greater benefit because of filters in the delay lock loop that round over the correlation peak. It is worth noting that in order to implement these values, the receiver needs a processor a speed of at least $\frac{1}{dT_c}$ Hz. T is the time over which measurements are averaged to yield a single solution; longer times typically yield better results, but if the receiver is moving quickly it might begin conflating measurements. Typical values range from 10 seconds in low-speed applications to 0.01-0.02 seconds for near-instantaneous measurements. Finally, the signal-to-noise ratio is comprised of many factors, but in the Earth environment usually falls in the bounds of Figure 9 (ignoring the “Determined threshold” line). These measurements were obtained over a 24-hour period in open sky conditions by Kubo et. al. [14] and represent baseline values from which to derive receiver noise; nominally, C/N_0 is in the region of 40 – 46 dB-Hz.

Since one chip width is the minimum position resolution obtainable by users, improving the clock rate onboard each node and subsequently reducing chip width can improve navigation accuracy from code measurements. Unfortunately, limitations may then begin to arise in receivers as required processing speed is at least $\frac{1}{dT_c}$ Hz.

Lunar Regolith

One large unknown on the lunar surface is the lunar regolith. Not much research has been done into its effects in radio signals; however, airborne particles from the regolith kicked up during takeoff or landing can attenuate signals if they are on a similar scale to the wavelength of the signal. Figure 10 plots the grain size distribution of the lunar

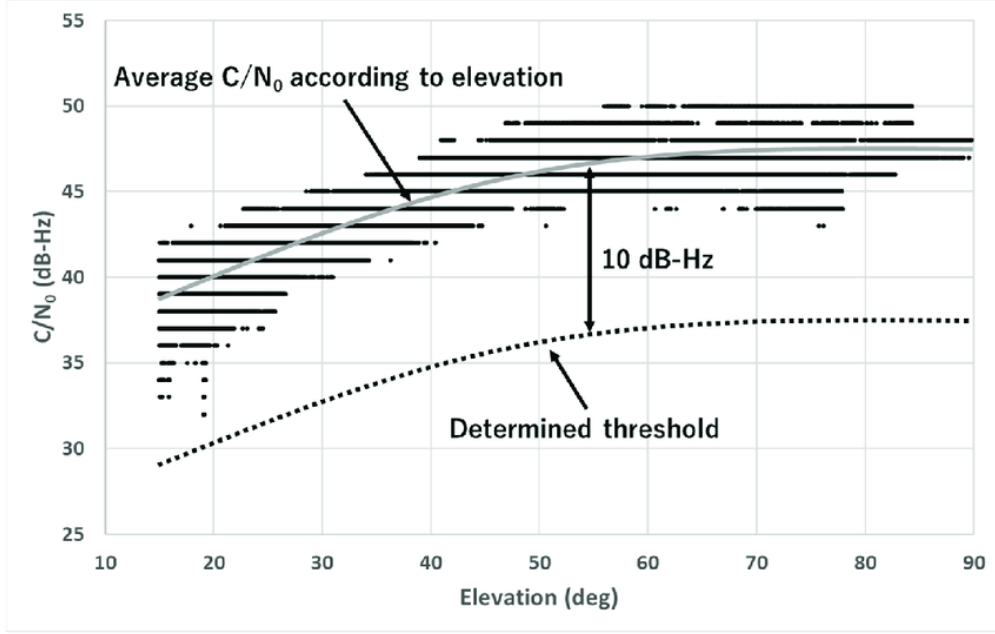


Fig. 9 C/N_0 versus elevation angle of GPS L1-C/A, open sky conditions [14].

regolith. Based on this data, most (> 99%) of regolith particles are under 5mm in grain size, which would then only attenuate signals on the order of 60 GHz or greater. Current LunaNet specifications target the 2483.5-2500MHz band for navigation signals, which is well beneath the attenuation threshold. A final consideration for the lunar regolith is its refractive index and potentially dispersive properties, similar to that of the ionosphere or troposphere. Literature available in this area is limited, but the error that arises is formulated as a path integral from the satellite to receiver[6, Chapter 5.3.1] as in Equation (8):

$$\Delta\tau = \frac{1}{c} \int_{\text{Satellite}}^{\text{Receiver}} [n(l) - 1] dl. \quad (8)$$

Here, c is the speed of light and $n(l)$ is a position-dependent refractive index of the media the wave is passing through. The refractive index also varies with the frequency of the signal passing through it – since the carrier and code are transmitted at different frequencies, this causes a phenomenon called code-carrier divergence. Around Earth, the ionosphere and troposphere are primary contributors; however, these stretch tens to hundreds of miles above the Earth’s surface, so waves transmitted by GNSS satellites travel through them often for hundreds of miles. If a similar phenomenon occurs in lunar regolith, it may only be for tens of meters and therefore impact the signal much less. In any case, this merits further research.

Finally, estimates of user navigation error (UNE) can be generated by synthesizing the resultant DOP based on current satellite geometry with clock and node OD errors, receiver noise, and multipath. Figure 11 depicts the user navigation error for the satellite constellations discussed in Section III. In all scenarios, it is assumed clock corrections are applied at t_0 .

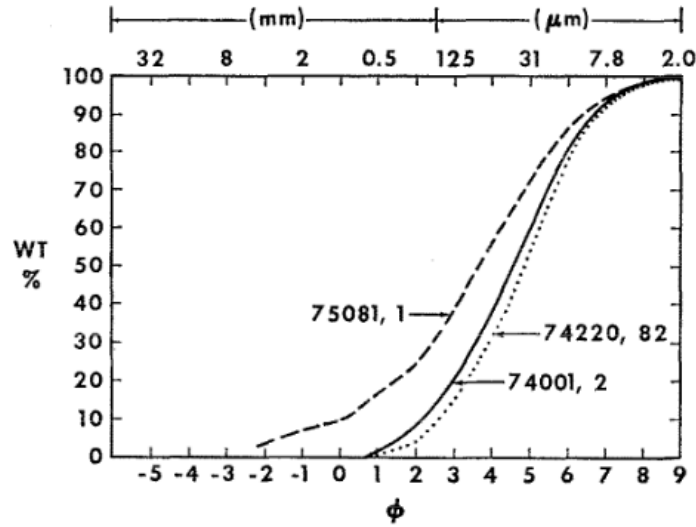
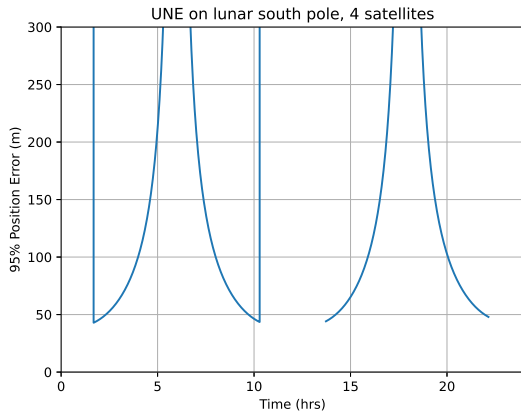


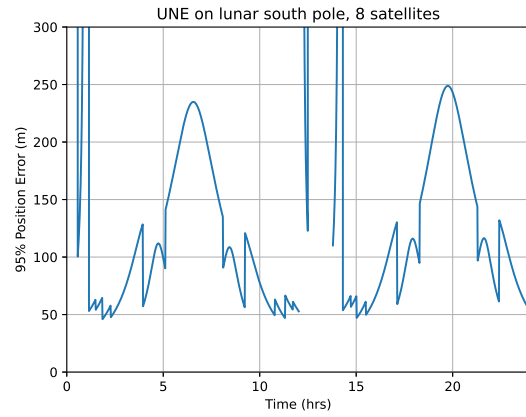
Fig. 10 Grain size distribution of mature lunar soil (75081) and orange soil (74220) [15].

These plots effectively illustrate the importance of multiple metrics for constellation evaluation. Figure 11c has comparatively much less error than Figure 11b when enough satellites are in view; however, the former experiences more coverage outages (periods of infinite error, e.g. not enough satellites in view). The time between outages is also more frequent for 11c. Ultimately, this means that if a lunar surface user was able to plan around the outages of the 5-satellite constellation and conduct operations requiring navigation within the 3-hour periods of coverage, that geometry would yield better navigation results. However, if longer durations of continuous coverage are required, the 8-satellite constellation would be more favorable. A more thorough discussion on these results can be found in Section V.

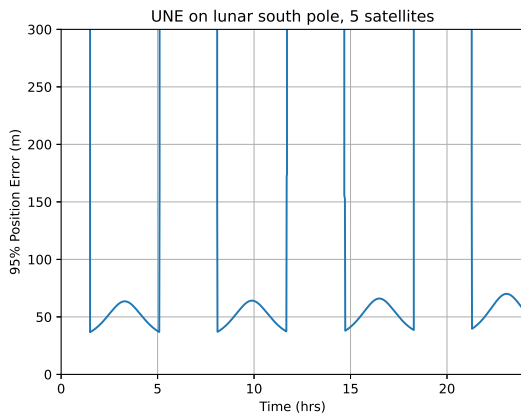
Table 1 gives some nominal values for 95% error bounds from the sources discussed above at a maximum Age-of-Data (AOD). If the clock model uncertainty is kept to the 30 ns bound mentioned previously, this would yield a maximum uncertainty of approximately 9 meters. Based on the orbit determination (OD) uncertainty computed through simulations in [13] which uses weak GNSS (accounting for outages at perilune), optical center-finding of the Moon, and a Rubidium standard, this would transfer an average uncertainty of 9 m to the user. Assuming a relatively benign multipath environment when compared to the Earth, a multipath error of roughly 2 m is reasonable.



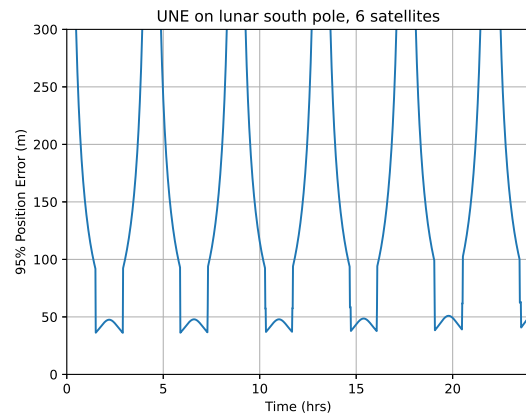
(a) 4-satellite constellation geometry.



(b) 8-satellite constellation geometry.



(c) 5-satellite constellation geometry.



(d) 6-satellite constellation geometry.

Fig. 11 95% UNE on lunar south pole using different constellation geometry.

Table 1 Collected error sources at maximum AOD.

Source	95% RSS Position Error
Clock Model	8.994 <i>m</i>
OD Uncertainty	9.081 <i>m</i>
Receiver Noise	19.818 <i>m</i>
Multipath	1.960 <i>m</i>
Lunar Regolith	0 <i>m</i>
Signal-In-Space Errors	12.931 <i>m</i>
Total	23.663 <i>m</i>

If the lunar regolith remains undisturbed and does not attenuate any of the signal, that results in a total signal-in-space error of 13 meters for the nominal LunaNet configuration based on the assumptions outlined above. Using a receiver with GPS-like C/N_0 and a low averaging time ($T = 0.02$ s) results in receiver noise of 20 m totalling a final UERE of 23.6 meters. This value for receiver noise is relatively high and can likely be driven lower with more modern receiver designs.

This section has outlined a tunable, programmatic approach for obtaining UERE and UNE given a sample constellation and various parameters about the setup. Section V will discuss in detail how this performance can be utilized by different users depending on their use case and phase of constellation deployment.

V. Navigation Performance

Choice of navigation algorithm will vary by user and operational phase based on their requirements. Current technologies are categorized as Phase 0; here, entities operating in cislunar space typically use a combination of Deep Space Network (DSN) ranging, weak GNSS [16], star-tracker measurements [17], and optical navigation center-finding or terrain-relative navigation [13] for measurements. Phase I will be characterized by deployment of navigation nodes to cover sites of interest like the lunar south pole; measurements using the constellation will be possible but coverage and availability will be limited. In this stage, there will be a couple options for users depending on requirements for timeliness of solution acquisition. If navigation solutions are not required in real-time, users can employ delayed estimation methods like batch estimation. Batch estimation is most useful for stationary users or with well-characterized dynamical trajectories; in this case, real-time navigation solutions would not be required. The benefits of a batch estimator like a linear unbiased minimum variance estimator are the ability to achieve more precise solutions and a resilience to service outages. However, many users such as lunar orbiters or rovers have uncertain dynamics and a need for real-time navigation solutions. Batch estimators may be infeasible as precise solutions are not available immediately and it becomes inaccurate to compute state transition matrices to align all measurements with a single time. In these cases, users are best served using real-time kinematic fixes or implementing a form of Kalman filter.

This section will analyze two lunar use cases: first, that of a ground station or other stationary user; second, a lunar rover that is equipped with an accelerometer and driving around with a somewhat uncertain trajectory for 24 hours – the uncertainty being characterized by an acceleration standard deviation of $\sigma_{\text{Rover}} = 3 * 10^{-7} \text{ m/s}^2$, selected to mimic performance of Mars rovers such as Perseverance and Curiosity. Both scenarios will be gathering position measurements from each of the four navigation constellations discussed in Section III, comparing the results between each.

A. Ground Station

Figures 13-16 depict 24-hour navigation simulations of a ground station placed at -75° latitude near the lunar south pole, shown in Figure 12. This stationary ground station is attempting to estimate its position on the lunar surface with

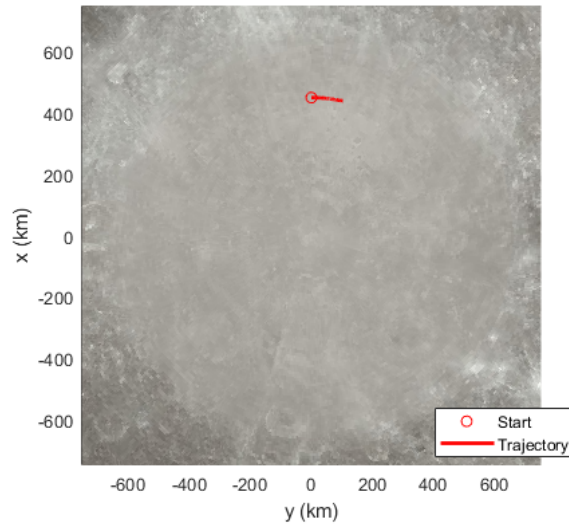


Fig. 12 Inertial trajectory of lunar ground station over 24 hours.

no *a priori* information using a batch filter (left) and an extended Kalman filter (right). Results are shown for each of the four constellation types and are summarized in Table 2.

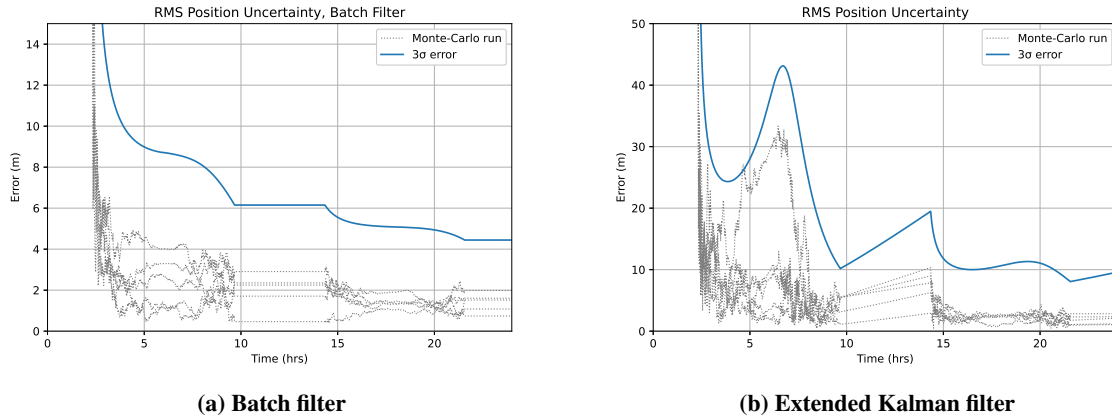
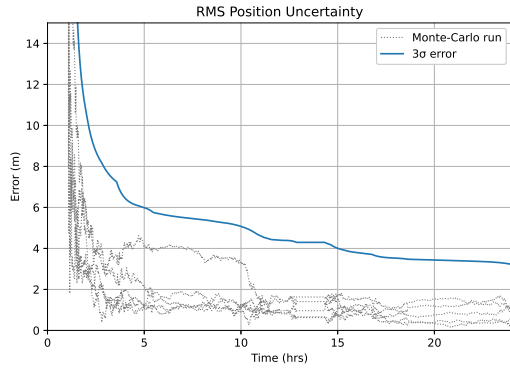


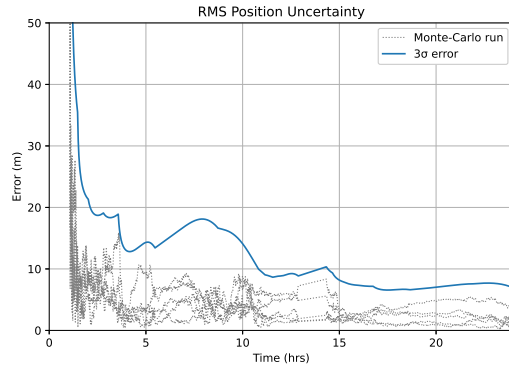
Fig. 13 Ground station navigating using the 4-satellite constellation.

Table 2 3σ RSS position error for the ground station after 24 hours using various methods.

Constellation	3σ error, Batch	3σ error, EKF
4-satellite	4.444 <i>m</i>	9.594 <i>m</i>
8-satellite	3.221 <i>m</i>	6.903 <i>m</i>
5-satellite	3.259 <i>m</i>	6.430 <i>m</i>
6-satellite	2.888 <i>m</i>	6.137 <i>m</i>

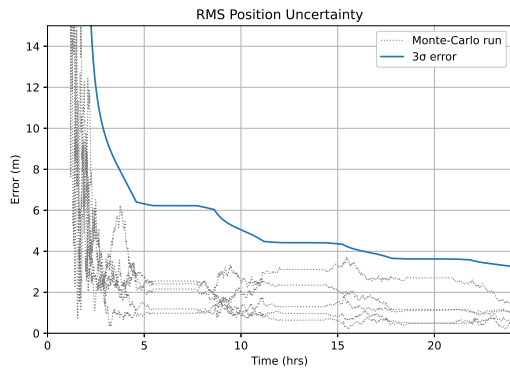


(a) Batch filter

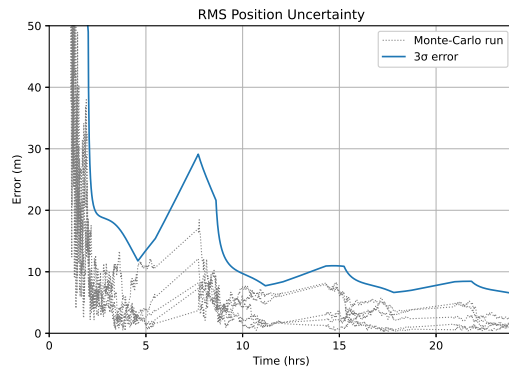


(b) Extended Kalman filter

Fig. 14 Ground station navigating using the 8-satellite constellation.



(a) Batch filter



(b) Extended Kalman filter

Fig. 15 Ground station navigating using the 5-satellite constellation.

Generally, the constellations from literature are characterized by having few service outages accompanied by long periods of coverage (as shown in Figure 11). However, the navigation error during these periods is generally much higher than the novel constellations. The result is that even with more frequent service outages in the 5- and 6-satellite constellations, it results in generally faster convergence to a solution when the system dynamics are well-known. Performance of the extended Kalman filter is slightly worse than the batch filter due to the real-time nature of the navigation solution and uncertainty accumulating during periods of navigation outages; however, the incorporation of system dynamics allows the filter to converge to a solution quicker than a batch filter.

B. Lunar Rover

Figures 18 and 19 depict 24-hour navigation simulations of a lunar surface rover following the trajectory depicted in Figure 17. This rover is driving around near the south pole and navigating using both the satellite constellation and an accelerometer in an extended Kalman filter.

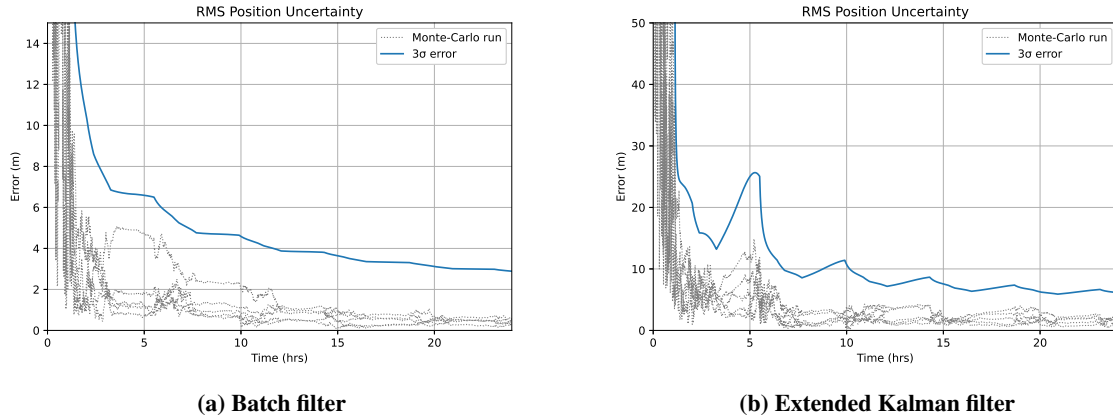


Fig. 16 Ground station navigating using the 6-satellite constellation.

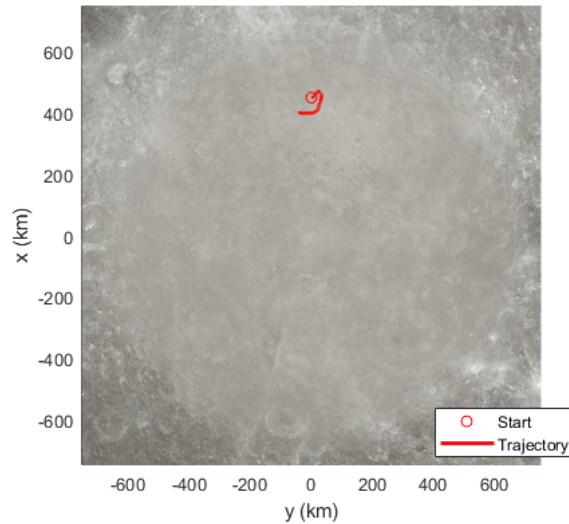
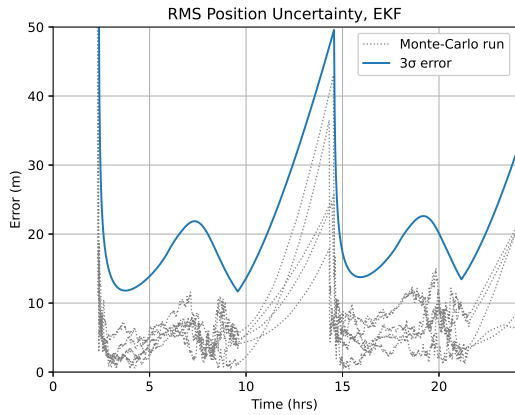


Fig. 17 Inertial trajectory of lunar rover over 24 hours.

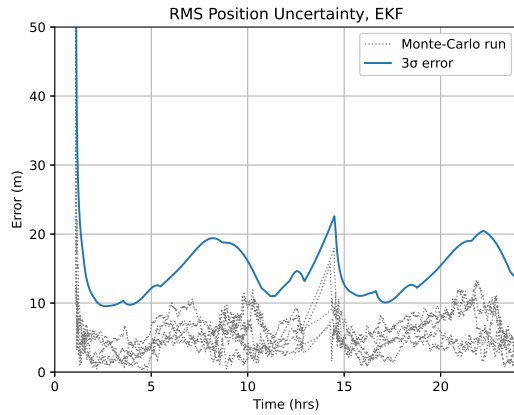
In these plots, error spikes are more severe than with the ground station as the dynamics are less certain since the rover is driving autonomously. As such, the constellations from literature – characterized by more prolonged periods of outages and higher average dilution of precision during periods of coverage – perform worse than the novel constellations. This is because the gap time between coverage is shorter than in the literature constellations and DOP is less on average; while there may be more gaps, their shorter nature allows the EKF to not spiral out of control as much and recover sooner once measurements are reacquired.

VI. Conclusions

This report details the reasoning behind selection of the method of navigation proposed (pseudorange-based trilateration), then steps through the derivation of user navigation error for a cislunar satellite navigation system akin to

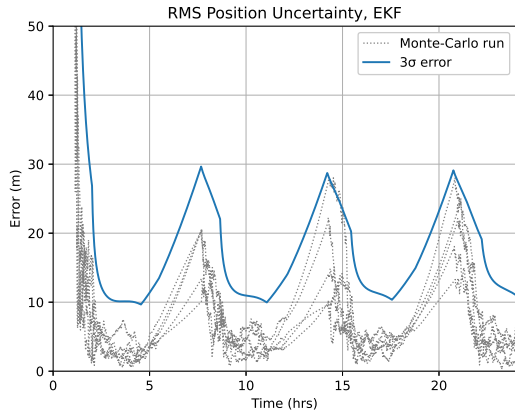


(a) EKF, 4-satellite constellation.

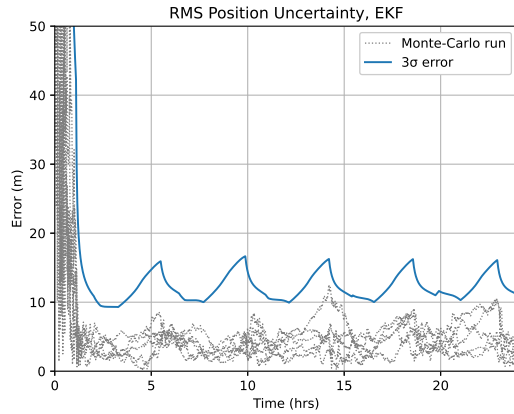


(b) EKF, 8-satellite constellation.

Fig. 18 Lunar surface rover navigating using constellations from literature.



(a) EKF, 5-satellite constellation.



(b) EKF, 6-satellite constellation.

Fig. 19 Lunar surface rover navigating using novel constellations.

Earth-based GNSS. Error sources such as the satellite node clock model, orbit determination uncertainty, receiver noise, multipath error, and lunar regolith are all considered to generate a 95% bound on the RSS position error of 23.663 meters (at the maximum age-of-data, which the moment just before node clock models are updated). This user equivalent range error, when combined with the individual constellation’s dilution of precision at the user’s location, yields a user navigation error that can be factored into simulations to determine the accuracy of navigation measurements.

Four early-stage lunar constellations are examined for providing navigation service to the lunar south pole – two from literature, and two novel constellations. These geometries are then compared across two case studies: the first being a 24-hour simulation of a lunar ground station navigating using a satellite constellation with these geometries; the second being similar, but instead with a mobile lunar rover. Results for each simulation are presented and navigation options such as batch and extended Kalman filters are explored. Tentatively, the software tool developed in this paper is capable

of providing valuable statistics and metrics across which multiple navigation system constellations can be evaluated.

Ultimately, this paper is part of broader work being completed for a GTRI internal research and development project to arrive at an optimal navigation system design and phasing plan. These objectives are currently of interest to the national and international community and will provide valuable insight for government organizations and companies – such as NASA, the ESA, and Intuitive Machines – invested in establishing lunar navigation systems.

References

- [1] Daniels, M., and Bretl, K., “National Cislunar Science & Technology Strategy,” , Nov. 2022. URL <https://www.whitehouse.gov/wp-content/uploads/2022/11/11-2022-NSTC-National-Cislunar-ST-Strategy.pdf>.
- [2] Goodliff, K., Merancy, N., Bhakta, S., Rucker, M., Chai, P. R.-P., Ashurst, T., Troutman, P., and Stromgren, C., “Moon-to-Mars Architecture Definition Document,” Tech. Rep. ESDMD-001, NASA, Apr. 2023.
- [3] Israel, D. J., Mauldin, K. D., Roberts, C. J., Mitchell, J. W., Pulkkinen, A. A., Cooper, L. V. D., Johnson, M. A., Christe, S. D., and Gramling, C. J., “LunaNet: a Flexible and Extensible Lunar Exploration Communications and Navigation Infrastructure,” *2020 IEEE Aerospace Conference*, IEEE, Big Sky, MT, USA, 2020, pp. 1–14. <https://doi.org/10.1109/AERO47225.2020.9172509>, URL <https://ieeexplore.ieee.org/document/9172509/>.
- [4] Giordano, P., Malman, F., Swinden, R., Zoccarato, P., and Ventura-Traveset, J., “The Lunar Pathfinder PNT Experiment and Moonlight Navigation Service: The Future of Lunar Position, Navigation and Timing,” Long Beach, California, 2022, pp. 632–642. <https://doi.org/10.33012/2022.18225>, URL <https://www.ion.org/publications/abstract.cfm?articleID=18225>.
- [5] Giorgi, G., Schmidt, T., Trainotti, C., Mata-Calvo, R., Fuchs, C., Hoque, M., Berdermann, J., Furthner, J., Günther, C., Schuldt, T., Sanjuan, J., Gohlke, M., Oswald, M., Braxmaier, C., Balidakis, K., Dick, G., Flechtner, F., Ge, M., Glaser, S., König, R., Michalak, G., Murböck, M., Semmling, M., and Schuh, H., “Advanced technologies for satellite navigation and geodesy,” *Advances in Space Research*, Vol. 64, No. 6, 2019, pp. 1256–1273. <https://doi.org/10.1016/j.asr.2019.06.010>, URL <https://linkinghub.elsevier.com/retrieve/pii/S0273117719304260>.
- [6] Misra, P., and Enge, P., *Global positioning system: signals, measurements, and performance*, 2nd ed., Ganga-Jamuna Press, Lincoln, Mass, 2006.
- [7] Israel, D., and Babu, N., “Draft LunaNet Interoperability Specification,” , Jul. 2022. URL <https://ntrs.nasa.gov/citations/20220010998>.
- [8] Bhamidipati, S., Mina, T., and Gao, G., “A Case Study Analysis for Designing a Lunar Navigation Satellite System with Time-Transfer from Earth-GPS,” Long Beach, California, 2022, pp. 407–419. <https://doi.org/10.33012/2022.18202>, URL <https://www.ion.org/publications/abstract.cfm?articleID=18202>.
- [9] Murata, M., Kawano, I., and Kogure, S., “Lunar Navigation Satellite System and Positioning Accuracy Evaluation,” Long Beach, California, 2022, pp. 582–586. <https://doi.org/10.33012/2022.18220>, URL <https://www.ion.org/publications/abstract.cfm?articleID=18220>.
- [10] Flores, A., and Nicholas, D., “NAVSTAR GPS Space Segment/Navigation User Interfaces,” , Apr. 2021. URL <https://www.gps.gov/technical/icwg/IS-GPS-200M.pdf>.
- [11] Moorefield, F., “Global Positioning System Standard Positioning Service Performance Standard,” , Apr. 2020.

- [12] Hustell, S. T., Reid, W. G., Crum, L. J. D., Mobbs, L. H. S., and Buisson, J. A., "Operational Use of the Hadamard variance in GPS," *Proceedings of the 28th Annual Precise Time and Time Interval Systems and Applications Meeting*, Reston, Virginia, 1996, pp. 201–214.
- [13] Small, J. L., Mann, L. M., Crenshaw, J. M., Gramling, C. J., Rosales, J. J., Winternitz, L. B., Hassouneh, M. A., Baker, D. A., Hur-Diaz, S., and Liounis, A. J., "Lunar Relay Onboard Navigation Performance and Effects on Lander Descent to Surface," Long Beach, California, 2022, pp. 587–601. <https://doi.org/10.33012/2022.18221>, URL <https://www.ion.org/publications/abstract.cfm?articleID=18221>.
- [14] Kubo, N., Kobayashi, K., and Furukawa, R., "GNSS Multipath Detection Using Continuous Time-Series C/N0," *Sensors*, Vol. 20, No. 14, 2020, p. 4059. <https://doi.org/10.3390/s20144059>, URL <https://www.mdpi.com/1424-8220/20/14/4059>.
- [15] Heiken, G. H., McKay, D. S., and Brown, R., "Lunar deposits of possible pyroclastic origin," *Geochimica et Cosmochimica Acta*, Vol. 38, No. 11, 1974, pp. 1703–1718. [https://doi.org/10.1016/0016-7037\(74\)90187-2](https://doi.org/10.1016/0016-7037(74)90187-2), URL <https://linkinghub.elsevier.com/retrieve/pii/0016703774901872>.
- [16] Locantore, J., and Gottifredi, F., "GNSS-Based Enhanced Precise Orbit Determination for the Moon Transfer Orbit," Long Beach, California, 2022, pp. 554–564. <https://doi.org/10.33012/2022.18215>, URL <https://www.ion.org/publications/abstract.cfm?articleID=18215>.
- [17] Critchley-Marrows, J. J., Wu, X., and Cairns, I. H., "Stellar Navigation on the Moon - A Compliment, Support and Back-up to Lunar Navigation," Long Beach, California, 2022, pp. 616–631. <https://doi.org/10.33012/2022.18177>, URL <https://www.ion.org/publications/abstract.cfm?articleID=18177>.